An Inductive Power Transfer Converter With High Efficiency Throughout Battery Charging Process

Zhicong Huang, *Member, IEEE,* Siu-Chung Wong, *Senior Member, IEEE,* and Chi K. Tse, *Fellow, IEEE*

Abstract

An inductive power transfer (IPT) converter usually has an optimum efficiency only at a matched load. Due to wide load range variation during battery charging, it is challenging for an IPT converter to achieve the required output and maintain high efficiency throughout the charging process. In this paper, a series-series compensated IPT (SSIPT) converter with an active rectifier is analyzed and implemented for battery charging. Appropriate operations are employed for constant current (CC) charging and constant voltage (CV) charging. A novel operation approach is proposed to achieve constant output voltage and ensure load impedance matching during CV charging without the help of an extra DC-DC converter which incurs loss. Either a frequency modulated primary inverter or a phase angle modulated secondary active rectifier can achieve soft switching. High efficiency can be maintained during the whole battery charging profile.

Index Terms

Inductive power transfer, Battery charging, Efficiency optimization, Soft switching.

I. Introduction

An inductive power transfer (IPT) system can transfer power wirelessly from a transmitter coil to a receiver coil over a short-range air gap which eliminates physical electrical contact between subsystems of the transmitter and receiver with minimal electromagnetic radiation [1]. With such a wireless convenience, IPT has been used for battery charging in many applications, such as consumer electronics, biomedical implants, electric vehicles, and so on [2]. Fig. 1 shows a typical charging profile of a battery, where the battery is charged initially by a constant current (CC) and subsequently by a constant voltage (CV) [3]. The charging process is started with CC charging at the rated value, where the battery voltage increases from the value of discharge cut-off to the value of charge threshold. The charging process is followed by the CV charging at the charge threshold voltage to fully charge the battery, where the charging current decreases from the rated value to the minimum value at only a few percent of the rated value. The equivalent DC resistance of the battery increases significantly during the charging process. With such a wide load range, the efficiency optimization is a challenging design problem for most converters.

In an IPT system, the transmitter coil and the receiver coil form a loosely coupled transformer which has significant leakage inductances and a relatively small mutual inductance. Compensation of reactive power from the transformer using external reactive elements is often required to improve system performances which may include power transfer capability, power efficiency, power regulation, and tolerance to misalignment between the coils [4]–[7]. The compensated transformer is often driven by an AC source generated from an inverter circuit for simplicity and good efficiency. An inverter circuit using half-bridge or full-bridge permits soft switching that significantly improves efficiency. Soft switching can be designed to achieve

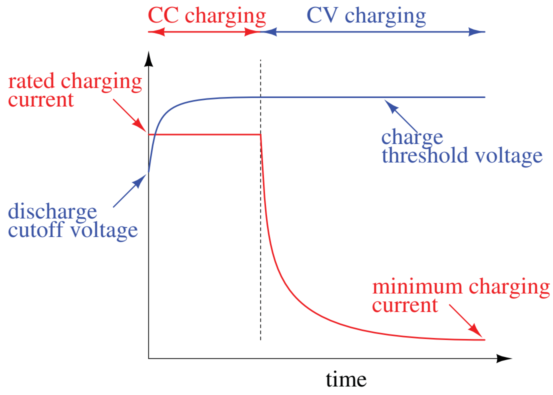

Fig. 1. Typical charging profile of a battery and operation modes of a battery charger.

TABLE I
DESIRABLE FEATURES OF AN IPT BATTERY CHARGER

Desirable feature	[12]–[14]	[15], [16]	[18], [23]	[19]–[22]	[24], [25]	[26], [27]
Efficiency optimization for wide load range	×	×	√	√	√	×
Soft switching of inverter and active rectifier circuits	√	√	√	√	×	√
No extra DC-DC converter	√	√	×	×	√	√
No extra power switch	×	√	√	√	√	√
Design for battery charging profile	√	√	√	√	√	×
Receiver side direct control	×	×	√	×	√	√

zero-voltage switch-on (ZVS) of MOSFET switches or zero-current switch-off (ZCS) of IGBT switches. Phase-shift pulse width modulation (PWM) control can be used to modulate the input for the required output in battery charging. However, soft switching is hard to achieve for even a small modulation depth. In order for the inverter circuit to achieve soft switching at a fixed duty cycle, DC-DC converters at the front-side and/or the load-side are/is often incorporated in an IPT system to perform the required modulation of power. As a trade off, maximum system efficiency suffers due to the use of more stages of power conversion. Alternatively, IPT converters can be designed at their native load-independent current (LIC) or load-independent voltage (LIV) output operating frequency [6], [8]–[11]. With the property of LIC or LIV, a very shallow duty cycle modulation can provide precise charging at CC or CV operation. Therefore, a converter stage can be saved.

The battery charging profile requires both CC and CV charging. Thus, a single IPT converter is designed with hybrid or switchable compensation topology to achieve both LIC and LIV output [12]–[14]. However, hybrid topologies need power switches in series with the power path that incur higher conduction loss and component cost. To reduce loss and cost, a single compensation topology can also be designed to operate at two operating frequencies for both the LIC and LIV output [15], [16].

The IPT converters mentioned above have the benefits of soft switching. They can be optimized for both CC and CV output with minimal control complexity. However, keeping the property of soft switching, they cannot be optimized for best efficiency using impedance matching without using a multistage design which includes front-side and load-side DC-DC converters [18]–[23]. Due to the wide range of battery DC resistance during CV charging, without impedance matching, the efficiency of the IPT converter degrades significantly, as demonstrated in [12]–[16].

In multistage designs, the load-side DC-DC converter transforms the load impedance into a matching load impedance to maintain maximum efficiency, while the front-end DC-DC converter modulates the input voltage amplitude of the IPT converter to control the input power. The IPT converter is always kept at optimal load and with soft switching. A wireless data feedback channel is normally required for the regulation of the output power. Different control schemes are studied, which include the minimum input current tracking [18], the maximum efficiency tracking [19]–[22] and the voltage ratio control [23]. The designs in [18], [23] use a receiver-side DC-DC converter for the direct control of output power such that fast wireless communication between the transmitter and receiver is not necessary. These *multistage* IPT systems with impedance matching for maximum system efficiency have obvious drawbacks. Losses and costs of additional DC-DC converters are inevitable. More complicated controllers are needed for the whole system and the additional DC-DC converters.

The additional DC-DC converters in *multistage* IPT systems apply modulation to achieve impedance matching which maintains the system at the optimal efficiency point without losing the soft switching property of the inverter. Alternatively, the modulation given by the additional DC-DC converter can be implemented by the inverter and active rectifier circuit as shown in Fig. 2. Thus, the extra DC-DC converters can be omitted. However, it has been shown directly in [15] and indirectly in [12]–[16] that deep PWM of the inverter suffers high loss due to hard switching. Nevertheless, disregarding switching losses from the inverter bridge and the active rectifier, impedance matching has been implemented in [24], [25]. In [24], [25], the modulation in the active rectifier ensures that the fundamental component of v_s and i_s are in phase, thus permitting direct application of the usual model for the fundamental frequency analysis.

Without the implementation of impedance matching for efficiency optimization for wide load range, soft switching of the active rectifier bridge is demonstrated in [26], [27]. A summary of desirable features for an IPT battery charger developed so far is given in Table I. It will be desirable to develop an IPT battery charger that has an optimized efficiency for wide load range applications in CV charging, soft switching of inverter and active rectifier circuits, no extra DC-DC converter, no extra power switch, design for the battery charging profile, and receiver side master control without the used of a fast wireless communication channel between the transmitter and receiver.

In this paper, we will develop an IPT battery charger as shown in Fig. 2 with all the desirable features desired in Table I. This paper is organized as follows. Section II highlights the system structure for battery charging and analyzes load impedance, voltage transfer ratio, efficiency and input impedance of the SSIPT converter with active rectifier. In Section III, critical criteria to achieve maximum efficiency is given for an arbitrary operating frequency, and a generally applicable load matching range is defined for maintaining a high system efficiency. Section IV proposes a novel approach to CV charging by controlling the operating frequency of the inverter and the conduction angle of the active rectifier. The output performance and efficiency performance are experimentally verified in Section V. Finally, Section VI concludes this paper.

II. System Structure and Theoretical Analysis

A. System Structure

In the schematic of an SSIPT converter shown in Fig. 2, the magnetic coupler has self inductances L_P and L_S, and mutual inductance M. Subscripts P and S indicate parameters in the primary and the secondary, respectively. The coupling coefficient

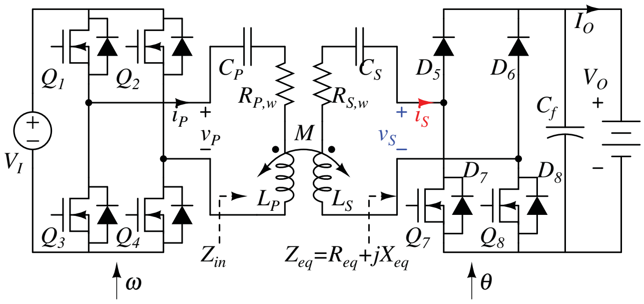

Fig. 2. Schematics of a series-series IPT (SSIPT) system.

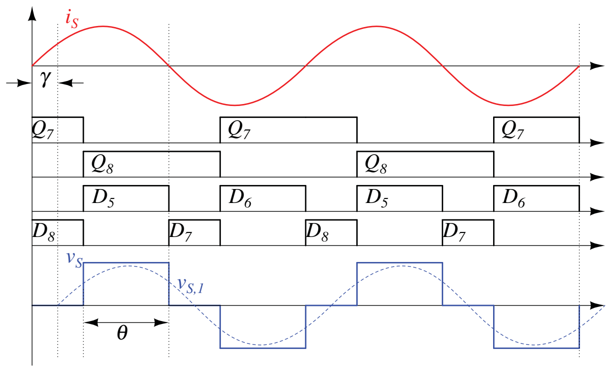

Fig. 3. Operation waveforms of the active rectifier.

is given by $k = \frac{M}{\sqrt{L_P L_S}}$. Both coils of the magnetic coupler are compensated by external capacitors C_P and C_S connected in series, with the resonant angular frequencies given by

$$\omega_P = \frac{1}{\sqrt{L_P C_P}}, \text{ and} \tag{1}$$

$$\omega_S = \frac{1}{\sqrt{L_S C_S}}. \tag{2}$$

Coil losses are represented by resistances $R_{P,w}$ and $R_{S,w}$. DC voltage source V_I is modulated to a high frequency AC voltage v_P which drives the primary coil through a full-bridge inverter having four MOSFETs Q_1–Q_4. The AC output is rectified to a DC output to charge the battery by an active rectifier with output filter capacitor C_f. Secondary AC voltage v_S and AC current i_S are the inputs of the active rectifier circuit. DC voltage V_O and current I_O are charging the battery. The active rectifier consists of two MOSFETs Q_7 and Q_8 and two diodes D_5 and D_6. Also, D_7 and D_8 are the anti-parallel diodes of Q_7 and Q_8.

B. Operating Waveforms and Equivalent Model

The operating waveforms of the active rectifier are shown in Fig. 3. Transistors Q_7 and Q_8 are turned on during the on time of their anti-parallel diodes in order to achieve ZVS. Both Q_7 and Q_8 are turned on for half a cycle. Therefore, Q_7 and Q_8 are turned off with a time delay of $\pi - \theta \in [0, \pi]$, until the zero cross points of i_S. Thus, the conduction angle θ of the active rectifier has maximum π and minimum 0. It should be noted that change of θ will affect the phase angle between v_S

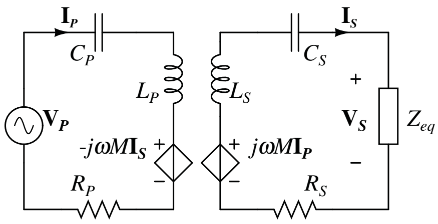

Fig. 4. AC equivalent circuit model of the SSIPT converter.

and i_S. As shown in Fig. 3, $v_{S,1}$ is the fundamental component of v_S, and it lags i_S with a phase angle given by $\gamma = \frac{\pi-\theta}{2}$. Therefore, the equivalent load is an impedance instead of the usual pure resistance.

Since the battery charging process is slow compared to the operating period of the SSIPT converter, the battery can be modeled as a resistor determined by the charging voltage and the charging current, i.e., $R_L = \frac{V_O}{I_O}$. It has been studied that the active rectifier together with resistive load can be represented by an equivalent fundamental impedance [26], [27], given by

$$Z_{eq} = R_{eq} + jX_{eq}, \tag{3}$$

where

$$R_{eq} = \frac{8}{\pi^2} R_L \sin^4\left(\frac{\theta}{2}\right), \text{ and} \tag{4}$$

$$X_{eq} = -\frac{8}{\pi^2} R_L \sin^3\left(\frac{\theta}{2}\right) \cos\left(\frac{\theta}{2}\right) \tag{5}$$

are the equivalent resistance and reactance, respectively.

Fig. 4 shows an equivalent model of the SSIPT converter using the fundamental approximation. This model is sufficiently accurate for high-quality resonant circuits operating near the resonant frequency. Here, $\mathbf{V}_P$, $\mathbf{I}_P$, $\mathbf{V}_S$ and $\mathbf{I}_S$ are phasors of the fundamental components of v_P, i_P, v_S and i_S, respectively. Resistor R_P includes losses from the primary coil and the inverter, while resistor R_S includes losses from the secondary coil and the active rectifier. The load is represented by an equivalent impedance Z_{eq} with resistance R_{eq} and reactance X_{eq}.

The basic equations for the circuit model in Fig. 4 are

$$(R_P + jX_P)\mathbf{I_P} - jX_M\mathbf{I}_S = \mathbf{V}_P, \tag{6}$$

$$-(R_S + R_{eq} + jX_S)\mathbf{I}_S + jX_M\mathbf{I}_P = 0. \tag{7}$$

where

$$X_M = \omega M, \tag{8}$$

$$X_P = \omega L_P - \frac{1}{\omega C_P}, \text{and} \tag{9}$$

$$X_S = \omega L_S - \frac{1}{\omega C_S} + X_{eq} \tag{10}$$

are the mutual reactance, the transmitter-side reactance and receiver-side reactance, respectively. The operating angular frequency is represented by ω. The input voltage of the active rectifier is given by $\mathbf{V}_S = (R_{eq} + jX_{eq})\mathbf{I}_S$.

C. Voltage Transfer Ratio, Power Efficiency and Input Impedance

Using Fourier analysis, the magnitudes of $\mathbf{V}_P$ and $\mathbf{V}_S$ are given by

$$|\mathbf{V}_P| = \frac{4}{\pi} V_I, \text{and} \tag{11}$$

$$|\mathbf{V}_S| = \frac{4}{\pi} \sin(\frac{\theta}{2}) V_O. \tag{12}$$

From (6)–(12), the DC voltage transfer ratio of the SSIPT converter shown in Fig. 2 can be calculated as

$$G_V = \frac{V_O}{V_I} \tag{13}$$

$$= \left| \frac{X_M \frac{Z_{eq}}{\sin(\frac{\theta}{2})}}{(R_P + jX_P)(R_S + R_{eq} + jX_S) + X_M^2} \right|. \tag{14}$$

Using the equivalent model shown in Fig. 4, the efficiency can be calculated by

$$\eta = \frac{|\mathbf{I}|_S^2 R_{eq}}{|\mathbf{I}|_S^2 R_{eq} + |\mathbf{I}|_S^2 R_S + |\mathbf{I}|_P^2 R_P} \tag{15}$$

$$= \frac{X_M^2 R_{eq}}{[(R_{eq} + R_S)^2 + X_S^2] R_P + X_M^2 (R_{eq} + R_S)}. \tag{16}$$

The input impedance and input phase angle can be found as

$$Z_{\text{in}} = R_P + jX_P + \frac{X_M^2}{R_{eq} + R_S + jX_S}, \text{ and} \tag{17}$$

$$\varphi = \frac{180}{\pi} \arctan \frac{\Re(Z_{\text{in}})}{\Im(Z_{\text{in}})}, \tag{18}$$

where $\Re(Z_{\text{in}})$ and $\Im(Z_{\text{in}})$ are the real and imaginary components of the input impedance Z_{in}, respectively.

III. Efficiency Optimization

A. Theoretical Maximum Efficiency

The power efficiency given in (16) can be simplified as

$$\eta \approx \frac{1}{\frac{R_{eq} + \frac{X_S^2}{R_{eq}}}{X_M^2} R_P + \frac{R_S}{R_{eq}} + 1} \tag{19}$$

with the assumptions $\frac{X_M^2}{R_P R_S} \gg 1$ and $\frac{R_{eq}}{R_S} > 1$.

We will find optimum values of R_{eq} and X_{eq} leading to maximum efficiency. For an arbitrary operating frequency ω, from (19), it is obvious that the efficiency can be maximized as

$$\eta_{\text{opt}} \approx \frac{1}{\frac{1}{k\sqrt{Q_P Q_S}} + 1}, \text{ if} \tag{20}$$

$$X_{S,\text{opt}} = \omega L_S - \frac{1}{\omega C_S} + X_{eq} = 0, \text{ and} \tag{21}$$

$$R_{eq,\text{opt}} = \omega M \sqrt{\frac{R_S}{R_P}}. \tag{22}$$

where $Q_P = \frac{\omega L_P}{R_P}$ and $Q_S = \frac{\omega L_S}{R_S}$ are quality factors of the primary and the secondary sides, respectively.

Equations (21) and (22) are the criteria of critical load impedance matching point that achieves maximum efficiency for an arbitrary operating frequency ω. Maximum efficiency η_{opt} in (20) is frequency-dependent. For near constant values of R_P

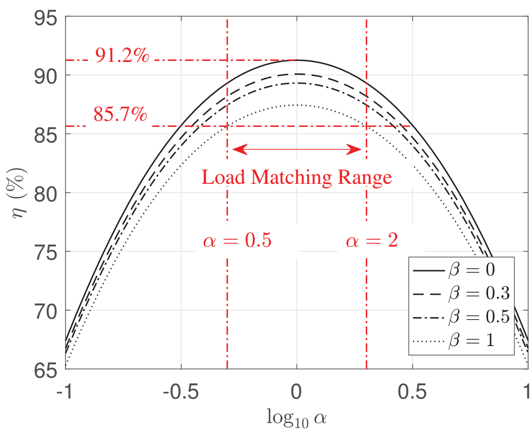

Fig. 5. Efficiency of the SSIPT converter versus $\log_{10} \alpha$.

TABLE II
SIMULATION PARAMETERS OF THE SSIPT CONVERTER FOR ANALYSIS

Parameters	Symbols	Values
Self inductance	L_P, L_S	118 μH, 172 μH
Coupling coefficient	k	0.283
Equivalent Resistance	R_P, R_S	0.5 mΩ, 0.72 mΩ
Compensation capacitance	C_P, C_S	85.865 nF, 58.908 nF
Resonant frequency	$\frac{\omega_P}{2\pi} = \frac{\omega_S}{2\pi}$	50 kHz

and R_S within a certain range of operating frequency, it is possible to achieve a higher efficiency as operating frequency ω increases, due to higher Q_P and Q_S.

B. Load Impedance Matching Range for Efficiency Optimization

Since the modulation of the active rectifier given in Fig. 3 cannot alter R_{eq} and X_{eq} independently, it is impractical for the SSIPT converter to operate at exactly $R_{eq,\text{opt}}$ and $X_{S,\text{opt}}$ in order to achieve maximum efficiency. We will find a range of R_{eq} and X_{eq} that gives an acceptable efficiency range. In doing so, we define a factor α representing the normalized R_{eq} with respect to $R_{eq,\text{opt}}$, i.e.,

$$\alpha = \frac{R_{eq}}{R_{eq,\text{opt}}}, \tag{23}$$

and a factor β representing the deviation of the normalized X_{eq} from 0, i.e.,

$$\beta = \frac{\frac{X_S^2}{R_{eq}}}{R_{eq,\text{opt}}}. \tag{24}$$

As an illustration, the efficiency of an SSIPT converter using parameters shown in Table II is plotted versus $\log_{10} \alpha$ at some values of $\beta < 1$ as shown in Fig. 5. A range of α and β can be selected for an acceptable minimum efficiency, say, 85.7%. Thus, $0.5 < \alpha < 2$ and $\beta < 1$ are selected. Unless specified otherwise, the parameters given in Table II will be used for the rest of this paper.

TABLE III
OPERATION OF THE SSIPT CONVERTER

Charging process	Operating frequency ω	Conduction angle θ
CC	ω_P	π
CV	Adjust according to optimal points shown in Fig. 9.	

IV. Design for Battery Charging

A. CC Charging

It is well known that an SSIPT converter can achieve LIC for CC charging at a high-efficiency point [5], [10], [13], [15]. The design methodology of the SSIPT converter with constant output current has been studied in [15], [28]. Since the range of battery resistance in CC charging is usually narrow, by locating the resistance range of CC charging within the load impedance matching range of the SSIPT converter, high efficiency can be achieve for CC charging, as shown by the red curve in Fig. 10(a). Precise output current is not necessary for CC charging. Therefore, the SSIPT converter can operate without any modulation, i.e., the active rectifier can operate similar to a passive rectifier with

$$\theta_{\mathrm{CC}} = \pi, \tag{25}$$

and the inverter can operate with high efficiency at a fixed frequency given by

$$\omega_{\mathrm{CC}} = \omega_P. \tag{26}$$

The operation of the SSIPT converter in CC charging is summarized in Table III.

Theoretically, if component losses are neglected, the output current is given by

$$I_O \approx \frac{8}{\pi^2}\frac{V_I}{\omega_P M}. \tag{27}$$

Substituting (22), (25) and (26) into (14), the output voltage at the load matching point can be found as

$$G_{V,\mathrm{opt}} \approx \sqrt{\frac{L_S}{L_P}}, \tag{28}$$

provided that component losses are neglected, and the load quality factors in the primary and the secondary are identical, i.e., $\frac{\omega L_P}{R_P} = \frac{\omega L_S}{R_S}$.

It should be noted that if primary resonant frequency ω_P and secondary resonant frequency ω_S are identical, input impedance Z_{in} of the SSIPT converter is purely resistive. To provide a slightly inductive input impedance for operating the primary inverter at ZVS, ω_P can be slightly lower than ω_S [15], [28].

B. CV Charging

For CV charging, precisely regulated output voltage is needed to charge the battery. An extra over-voltage protection is usually implemented for safe operation. The efficiency of the SSIPT converter should also be optimized by impedance transformation for the wide load range of CV charging. For the SSIPT converter with active rectifier shown in Fig. 2, we have two independent control parameters, which are

- the operating frequency ω of the inverter, and

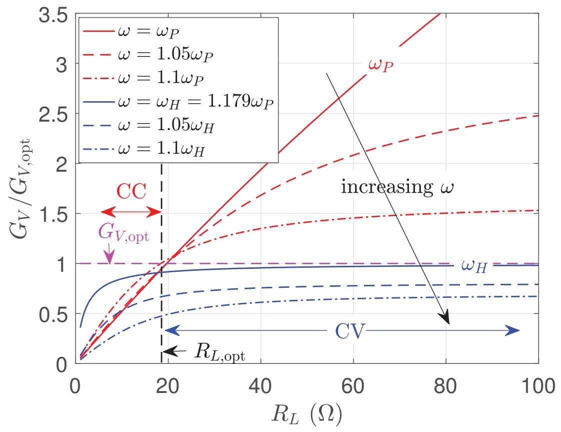

Fig. 6. Voltage transfer ratio versus load resistance under various operating frequencies.

- the conduction angle θ of the active rectifier.

Although we can readily achieve constant voltage output by controlling ω and θ, we first restrict the range of ω by considering over-voltage protection. The charging power will keep increasing during CC charging until the battery voltage reaches the charge threshold value. At the point of reaching the maximum charging power, it is safer for the inverter to switch to another operating frequency, where over-voltage will not happen, even if there is no control in the secondary active rectifier. Fig. 6 shows the voltage transfer ratio versus load resistance under different operating frequencies. In CC charging, the SSIPT converter operates at ω_P to achieve constant output current, as the solid red curve shows. In CV charging, if the operating frequency is above ω_H, the voltage transfer ratio G_V will always be smaller than $G_{V,\text{opt}}$, as the solid blue curve and dashed magenta curve show. Frequency $\omega_H = \frac{\omega_P}{\sqrt{1-k}}$ is the operating frequency of the SSIPT converter at which an LIV output is achieved [15]. Therefore, we can switch the operating frequency from ω_P to ω_H once maximum charging power is reached for a safe charging operation. During CV charging, control of ω will start from ω_H.

Since winding loss and converter loss are inevitable, practical voltage transfer ratio G_V will always be smaller than $G_{V,\text{opt}} = \sqrt{\frac{L_S}{L_P}}$. Specifically, G_V is designed at $0.9\sqrt{\frac{L_S}{L_P}} \approx 1.09$ as an example. Fig. 7 shows variation of voltage transfer ratio G_V versus operating frequency ω and conduction angle θ under different load conditions. The operating points $\{(\omega,\theta)\}$ for achieving $G_V = 1.09$ are plotted in three-dimensional space as red curves shown in Fig. 7 under different loading conditions. Fig. 8 shows the corresponding variation of efficiency η. Among these operating points $\{(\omega,\theta)\}$, we can identify the locations in the load impedance matching range, as illustrated in Fig. 5, to achieve a constant output voltage with high efficiency.

Therefore, a two-step procedure can be carried out to derive the operating points for CV charging by using a numerical calculation tool such as Matlab.

1) Given a constant G_V, solve (14) to find all the solutions $A_i\{(\omega,\theta)\}$ for each load $R_{L,i}$ in CV charging, where $\omega > \omega_H$ and $0 < \theta < \pi$ are the constraints.
2) Substitute $A_i\{(\omega,\theta)\}$ into (16) and search for the maximum efficiency, and find the optimum operation points $A_i(\omega_{\text{CV}},\theta_{\text{CV}})$ for each load $R_{L,i}$ in CV charging.

With these numerical solutions, the operating points in the load impedance matching range can be found to achieve constant

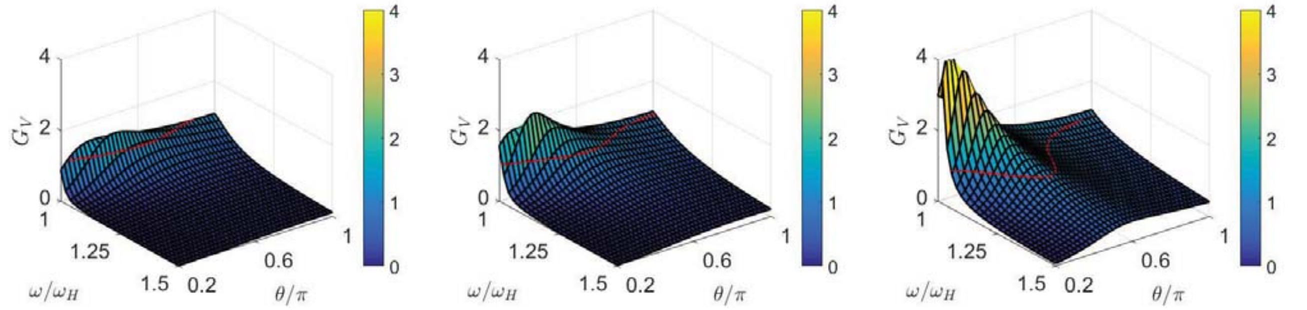

(a) (b) (c)

Fig. 7. Variation of voltage transfer ratio G_V with respect to operating frequency ω and conduction angle θ for (a) $R_L = 10\ \Omega$, (b) $R_L = 30\ \Omega$ and (c) $R_L = 100\ \Omega$.

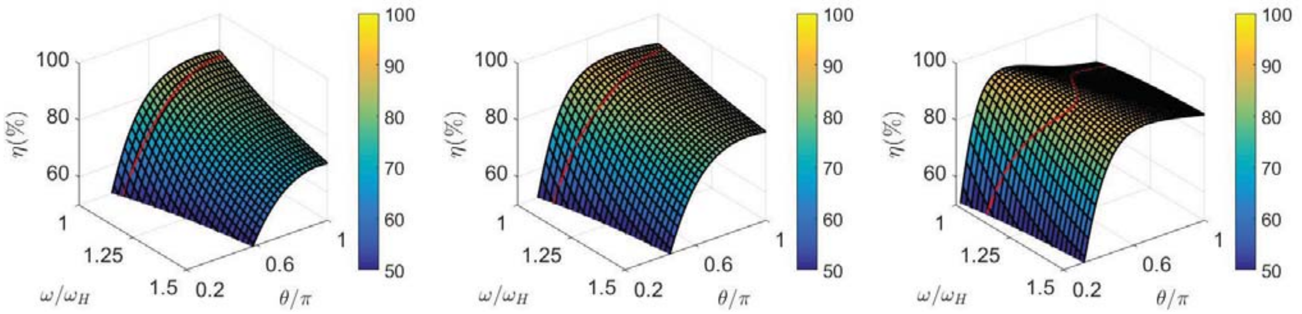

(a) (b) (c)

Fig. 8. Variation of efficiency η with respect to operating frequency ω and conduction angle θ for (a) $R_L = 10\ \Omega$, (b) $R_L = 30\ \Omega$ and (c) $R_L = 100\ \Omega$.

voltage output. Fig. 9 demonstrates the solution in a two-dimensional space. Solid curves in different colors represent possible solutions to achieve constant G_V for different load conditions. Points marked with "x" are the optimum operating points having maximum efficiency, for R_L varying from $15\ \Omega$ to $160\ \Omega$ as indicated by the arrow direction.

Since battery charging is a slow process, the dynamic response is not a critical issue for efficiency optimization. It is feasible to implement the control with the optimum operating point set at (ω, θ), as shown in Fig. 9, by using entries of R_L through lookup table. By controlling ω and θ, the SSIPT converter can achieve a fast and precise control of constant output voltage by modulating θ in the receiver side for CV charging. The information of loading resistance can be fed back to the transmitter side wirelessly to maintain a high efficiency during the whole CV charging process.

C. Comparison of Efficiency and Load Impedance

Efficiency comparison between the SSIPT converter designed with the conventional approach in [15], which does not have efficiency optimization for wide load range during CV charging, and the SSIPT converter developed in this paper will be given in this subsection. As shown in Fig. 10(a), the efficiency degrades significantly as the battery resistance increases rapidly during CV charging, due to mismatch in the load impedance. Based on the proposed approach in Section IV-B, the novel SSIPT converter can achieve constant output voltage for CV charging, with the ability to transform load impedance within a matching range. The efficiency is kept high as shown by the blue solid curve or blue-dash curve in Fig. 10(a). The blue solid

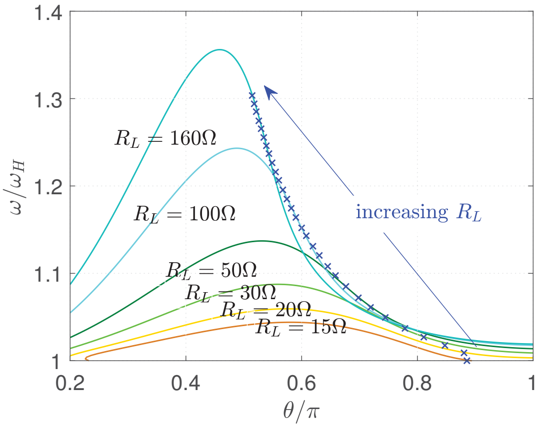

Fig. 9. Numerical solutions shown as a curve for some selected load resistances to achieve a constant $G_V = 1.09$, and optimum operating points shown as "x" to have high efficiency.

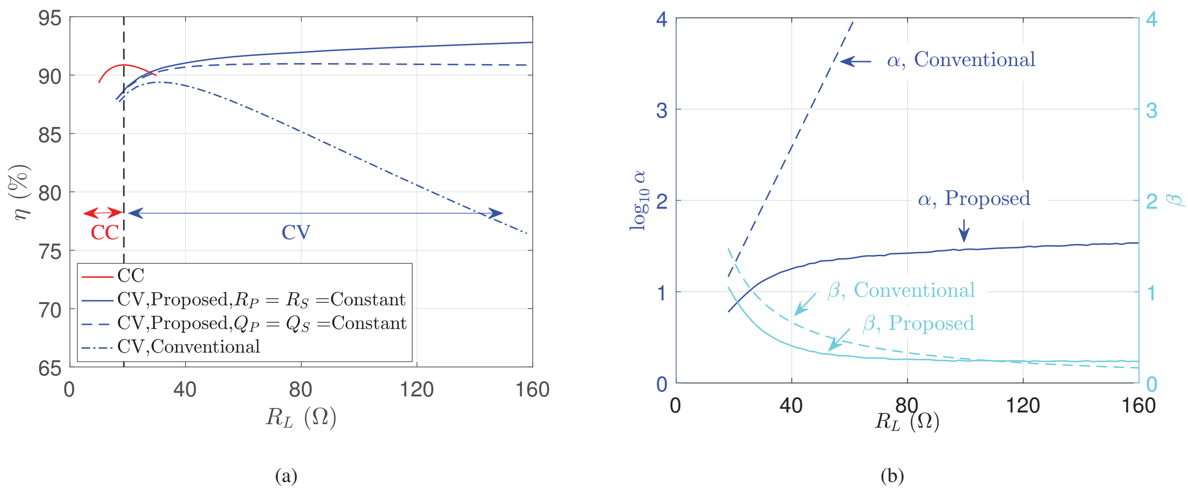

Fig. 10. Comparisons between the proposed approach in this paper and the conventional approach in [15] for (a) efficiency, and (b) α and β versus R_L.

curve is obtained by simulation with constant resistance $R_P = R_S$, while the blue-dash-dot curve corresponds to constant quality factor $Q_P = Q_S$.

As discussed in Section III-B, a load matching range can be defined by $0.5 < \alpha < 2$ and $\beta < 1$. It can be observed in Fig. 10(b) that the load impedance is located within a matching range when using the proposed approach, as the solid blue curve and the solid cyan curve show. However, as a comparison, the load resistance of the conventional approach deviates from the matching range significantly as shown by the blue dash curve in Fig. 10(b).

D. Soft Switching

In CV charging, the operation of the secondary active rectifier can achieve ZVS as discussed in Section II-B. Substituting the operating points $A_i(\omega_{\rm CV}, \theta_{\rm CV})$ into (17), the input impedance can be calculated. With (18), input phase angle φ is plotted in Fig. 11. Since φ is always positive, the primary inverter can always operate at ZVS during the whole CV charging process.

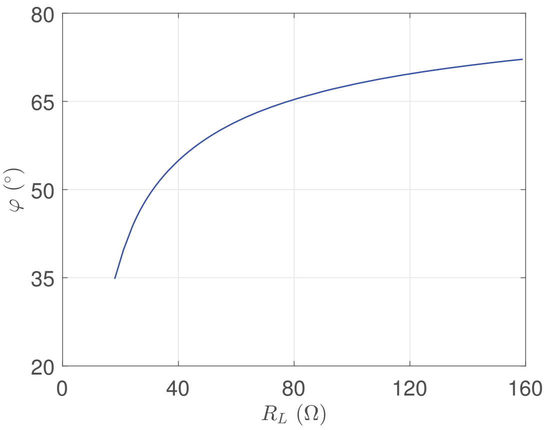

Fig. 11. Input phase angle of the SSIPT converter during CV charging process.

TABLE IV
CHARGING SPECIFICATIONS

Charging Specifications	Values
Discharge cut-off voltage	36 V
Charge threshold voltage	52 V
Rated charge current	3A
Minimum charge current	0.3A

V. EXPERIMENTAL VERIFICATION

A. Experimental Prototype

To verify the efficiency performance of the proposed approach, an experimental prototype is built with the schematic shown in Fig. 2. According to the charging profile shown in Fig. 1 and its specifications given in Table IV, the battery resistance ranges from 12 Ω to 17.3 Ω for CC charging and 17.3 Ω to 173 Ω for CV charging. System parameters are given in Table V. An electronic load is used to emulate the equivalent resistance of the battery.

TABLE V
SYSTEM PARAMETERS

System Parameters	Symbols	Values
Input voltage	V_I	50V
Switch	Q_1-Q_8, D_5-D_6	IPP60R165, MBR20200
Self inductance	L_P, L_S	117.6 μH, 172.7 μH
Coupling coefficient	k	0.283
Coil resistance	$R_{P,w}$, $R_{S,w}$	0.41 mΩ, 0.54 mΩ
Compensation capacitance	C_P, C_S	86.22 nF, 56.04 nF
Resonant frequency	$\frac{\omega_P}{2\pi}$, $\frac{\omega_S}{2\pi}$	49.98 kHz, 51.16 kHz

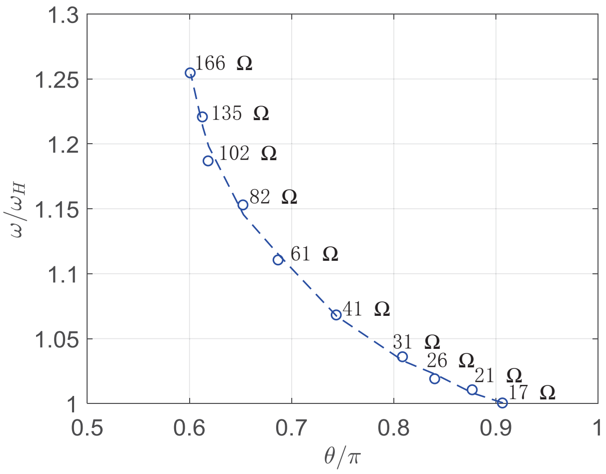

Fig. 12. Measured operating points at a fixed voltage output of 52 V and the corresponding load resistances.

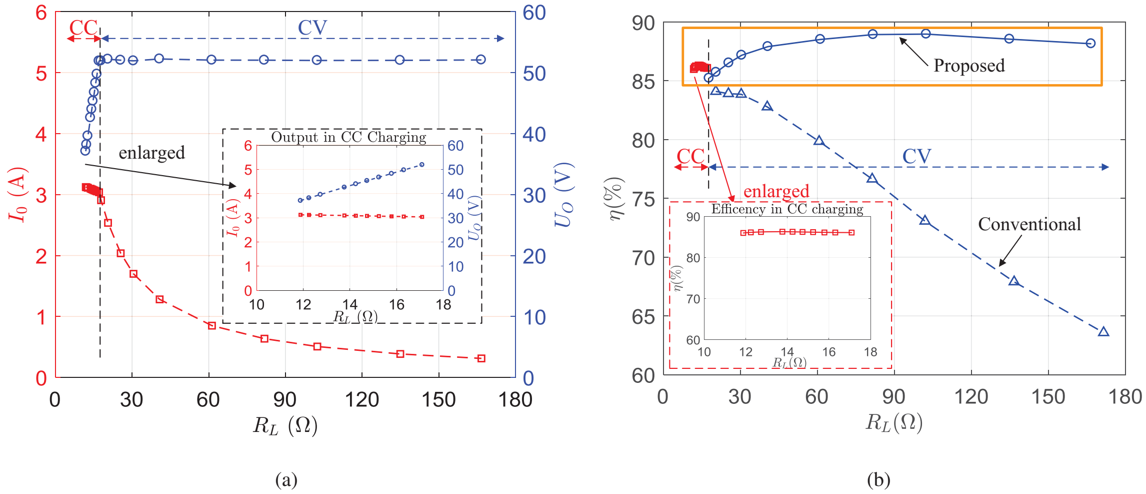

Fig. 13. (a) Measured output current and voltage versus battery resistance. (b) Measured efficiency versus battery resistance.

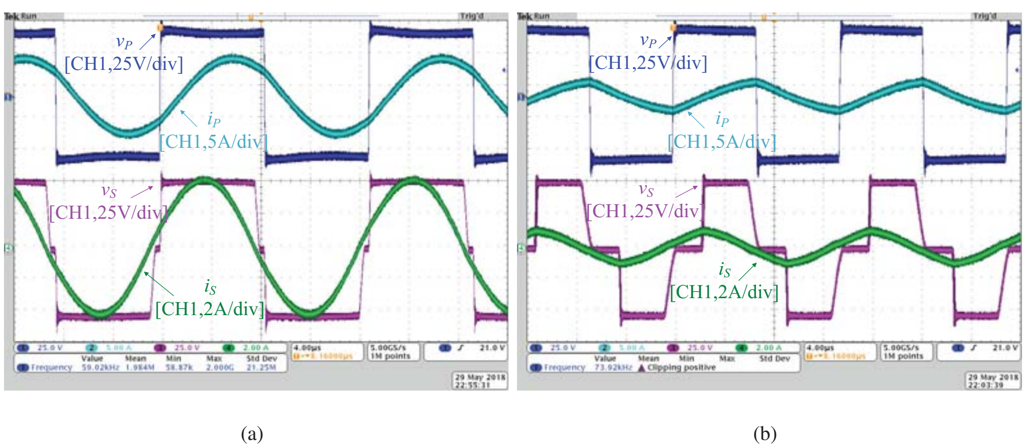

Fig. 14. Waveforms of the inverter and the active rectifier circuits at (a) the start and (b) the end of CV charging.

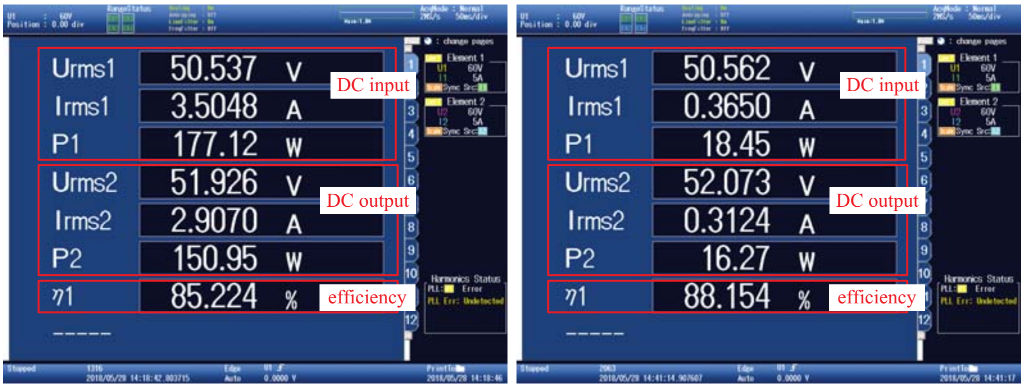

(a) (b)

Fig. 15. Screen capture of efficiency measurement at (a) the start and (b) the end of CV charging.

B. Measured Operating Points, Efficiency and Waveforms

First, the active rectifier operates as a passive rectifier, and the inverter operates at $\frac{\omega_P}{2\pi} = 49.98$ kHz to achieve native LIC for CC charging. Measured output current points (marked with "□") are shown in Fig. 13(a). It can be observed that the output current is nearly constant at 3 A, which satisfies the requirement of CC charging. Second, after the battery voltage reaches 52 V, CV charging should be employed. Following the proposed operation approach in Section IV-B, conduction angle θ of the active rectifier and operating frequency ω of the inverter are adjusted to achieve constant voltage output with optimum efficiency performance. The measured operating points (marked with "◯") are shown in Fig. 12, with ω and θ varying from 59 kHz to 74 kHz and from 168° to 108°, respectively. The corresponding output voltages (marked with "◯") are kept at 52 V, as shown in Fig. 13(a). The output voltage satisfies the requirement of CV charging.

The input DC power and output DC power are measured by a Yokogawa PX8000 Precision Power Scope. The measured efficiency points of the whole charging process are shown in Fig. 13, within the highlighted orange box. Efficiency points of CC charging (marked with "□") are about 86%. The measured efficiency points of CV charging (marked with "◯") are from 85% to 89%. As a comparison, the measured efficiency points (marked with "△") using the conventional approach [15] to achieve constant output voltage are also shown in Fig. 13, which decreases significantly as the battery resistance increases. To sum up, a high efficiency can be maintained for the whole charging process by using the proposed approach. The higher efficiency during the CV charging than the CC charging is attributed to the reduced conduction loss of using active rectifier and the higher quality factors of the transformer coils at higher operating frequencies.

Waveforms of the inverter and the active rectifier at the start and end of CV charging are shown in Fig. 14(a) and Fig. 14(b), respectively. It can be observed that ZVS is achievable in both the inverter and the active rectifier. Efficiency measurements at the start and end of CV charging are shown in Fig. 15(a) and Fig. 15(b), respectively.

VI. Conclusion

An SSIPT battery charger that permits efficiency optimization for a wide load range, soft switching of inverter and active rectifier circuits, no extra DC-DC converter, no extra power switch and receiver side direct control, is analyzed and implemented in this paper. Different operations are employed for constant current charging and constant voltage charging. A novel operation approach is proposed to achieve constant output voltage and ensure load impedance matching during constant voltage charging, by controlling the operating frequency of the primary inverter and the conduction angle of the secondary active rectifier. A high efficiency can be maintained for the whole battery charging process.

REFERENCES

[1] S. Y. R. Hui, W. Zhong and C. K. Lee, "A critical review of recent progress in mid-range wireless power transfer,' *IEEE Trans. Power Electron.,* vol. 29, no. 9, pp. 4500–4511, Sep. 2014.

[2] G. A. Covic and J. T. Boys, "Inductive power transfer," *Proc. IEEE,* vol. 101, no. 6, pp. 1276–1289, Jun. 2013.

[3] A. A. Hussein and I. Batarseh, "A review of charging algorithms for nickel and lithium battery chargers," *IEEE Trans. Veh. Technol.,* vol. 60, no. 3, pp. 830–838, Mar. 2011.

[4] C. S. Wang, G. A. Covic and O. H. Stielau, "Power transfer capability and bifurcation phenomena of loosely coupled inductive power transfer systems" *IEEE Trans. on Ind. Electron.,* vol. 51, no. 1, pp. 148–157, Feb. 2004.

[5] Y. H. Sohn, B. H. Choi, E. S. Lee, G. C. Lim, G. H. Cho and C. T. Rim, "General unified analyses of two-capacitor inductive power transfer systems: equivalence of current-source SS and SP compensations," *IEEE Trans. Power Electron.,* vol. 30, no. 11, pp. 6030–6045, Nov. 2015.

[6] W. Zhang and C. C. Mi, "Compensation topologies of high-power wireless power transfer systems," *IEEE Trans. Veh. Technol.,* vol. 65, no. 6, pp. 4768–4778, Jun. 2016.

[7] J. L. Villa, J. Sallan, J. F. S. Osorio and A. Llombart, "High-misalignment tolerant compensation topology for ICPT systems," *IEEE Trans. on Ind. Electron.,* vol. 59, no. 2, pp. 945–951, Feb. 2012.

[8] W. Zhang, S. C. Wong, C. K. Tse and Q. Chen, "Design for efficiency optimization and voltage controllability of series–series compensated inductive power transfer systems," *IEEE Trans. Power Electron.,* vol. 29, no. 1, pp. 191–200, Jan. 2014.

[9] W. Zhang, S. C.Wong, C. K. Tse, and Q. Chen, "Analysis and comparison of secondary series and parallel compensated inductive power transfer systems operating for optimal efficiency and load-independent voltage transfer ratio," *IEEE Trans. Power Electron.,* vol. 29, no. 6, pp. 2979–2990, Jun. 2014.

[10] W. Zhang, S. C.Wong, C. K. Tse, and Q. Chen, "Load-independent duality of current and voltage outputs of a series or parallel compensated inductive power transfer converter with optimized efficiency," *IEEE J. Emerg. Sel. Topics. Power Electron.,* vol. 3, no. 1, pp. 137–146, Mar. 2015.

[11] S. Samanta and A. K. Rathore, "Analysis and design of load-independent ZPA operation for P/S, PS/S, P/SP, and PS/SP tank networks in IPT applications," *IEEE Trans. Power Electron.,* vol. 33, no. 8, pp. 6476–6482, Aug. 2018.

[12] C. Auvigne, P. Germano, D. Ladas and Y. Perriard, "A dual-topology ICPT applied to an electric vehicle battery charger," in *Proc. Int. Conf. Electr. Mach.,* Mar., 2012, pp. 2287–2292.

[13] X. Qu, H. Han, S. C. Wong, C. K. Tse and W. Chen, "Hybrid IPT topologies with constant current or constant voltage output for battery charging applications," *IEEE Trans. Power Electron.,* vol. 30, no. 11, pp. 6329–6337, Nov. 2015.

[14] R. Mai, Y. Chen, Y. Li, Y. Zhang, G. Cao and Z. He, "Inductive power transfer for massive electric bicycles charging based on hybrid topology switching with a single inverter," *IEEE Trans. Power Electron.,* vol. 32, no. 8, pp. 5897–5906, Aug. 2017.

[15] Z. Huang, S. C. Wong and C. K. Tse, "Design of a single-stage inductive-power-transfer converter for efficient EV battery charging," *IEEE Trans. Veh. Technol.,* vol. 66, no. 7, pp. 5808–5821, Jul. 2017.

[16] V. B. Vu, D. H. Tran and W. Choi, "Implementation of the constant current and constant voltage charge of inductive power transfer systems with the double-sided LCC compensation topology for electric vehicle battery charge applications," *IEEE Trans. Power Electron.,* doi: 10.1109/TPEL.2017.2766605

[17] W. Zhong and S. Y. Hui, "Reconfigurable wireless power transfer systems with high energy efficiency over wide load range," *IEEE Trans. Power Electron.,* vol. 33, no. 7, pp. 6379–6390, Jul. 2018.

[18] W. X. Zhong and S. Y. R. Hui, "Maximum energy efficiency tracking for wireless power transfer systems," *IEEE Trans. Power Electron.,* vol. 30, no. 7, pp. 4025–4034, Jul. 2015.

[19] M. Fu, C. Ma, and X. Zhu, "A cascaded boost-buck converter for high efficiency wireless power transfer systems," *IEEE Trans. Ind. Informat.,* vol. 10, no. 3, pp. 1972–1980, Aug. 2014.

[20] M. Fu, H. Yin, X. Zhu, and C.Ma, "Analysis and tracking of optimal load in wireless power transfer systems," *IEEE Trans. Power Electron.,* vol. 30, no. 7, pp. 3952–3963, Jul. 2015.

[21] H. Li, J. Li, K. Wang, W. Chen, and X. Yang, "A maximum efficiency point tracking control scheme for wireless power transfer systems using magnetic resonant coupling," *IEEE Trans. Power Electron.,* vol. 30, no. 7, pp. 3998–4008, Jul. 2015.

[22] T. D. Yeo, D. Kwon, S. T. Khang, and J. W. Yu, "Design of maximum efficiency tracking control scheme for closed-loop wireless power charging system employing series resonant tank," *IEEE Trans. Power Electron.,* vol. 32, no. 1, pp. 471–478, Jan. 2017.

[23] Z. Huang, S. C. Wong and C. K. Tse, “Control Design for Optimizing Efficiency in Inductive Power Transfer Systems,” *IEEE Trans. Power Electron.,* vol. 33, no. 5, pp. 4523–4534, May 2018.

[24] T. Diekhans and R. W. De Doncker, “A dual-side controlled inductive power transfer system optimized for large coupling factor variations and partial load,” *IEEE Trans. Power Electron.,* vol. 30, no. 11, pp. 6320–6328, Nov. 2015.

[25] Z. Li, K. Song, J. Jiang and C. Zhu, “Constant current charging and maximum efficiency tracking control scheme for supercapacitor wireless charging,” *IEEE Trans. Power Electron.,* doi: 10.1109/TPEL.2018.2793312

[26] Q. Chen, L. Jiang, J. Hou, X. Ren and X. Ruan, “Research on bidirectional contactless resonant converter for energy charging between EVs,” *in Proc. 39th Annu. Conf. IEEE Ind. Electron. Soc.,* Vienna, Nov. 2013, pp. 1236–1241.

[27] K. Colak, E. Asa, M. Bojarski, D. Czarkowski and O. C. Onar, “A novel phase-shift control of semibridgeless active rectifier for wireless power transfer,” *IEEE Trans. Power Electron.,* vol. 30, no. 11, pp. 6288–6297, Nov. 2015.

[28] X. Qu, W. Zhang, S. C. Wong and C. K. Tse, “Design of a current-source-output inductive power transfer LED lighting system,” *IEEE J. Emerg. Sel. Topics Power Electron.,* vol. 3, no. 1, pp. 306–314, Mar. 2015.